Journal Pre-proofs



Experimental study of a single char particle combustion characteristics in a fluidized bed under O_2/H_2O condition

Lin Li, Lunbo Duan, Zhihao Yang, Shuai Tong, Edward John Anthony, Changsui Zhao

PII: S1385-8947(19)32352-6
DOI: https://doi.org/10.1016/j.cej.2019.122942
Reference: CEJ 122942

To appear in: *Chemical Engineering Journal*

Received Date: 4 June 2019
Revised Date: 19 September 2019
Accepted Date: 22 September 2019

Please cite this article as: L. Li, L. Duan, Z. Yang, S. Tong, E. John Anthony, C. Zhao, Experimental study of a single char particle combustion characteristics in a fluidized bed under O_2/H_2O condition, *Chemical Engineering Journal* (2019), doi: https://doi.org/10.1016/j.cej.2019.122942

This is a PDF file of an article that has undergone enhancements after acceptance, such as the addition of a cover page and metadata, and formatting for readability, but it is not yet the definitive version of record. This version will undergo additional copyediting, typesetting and review before it is published in its final form, but we are providing this version to give early visibility of the article. Please note that, during the production process, errors may be discovered which could affect the content, and all legal disclaimers that apply to the journal pertain.

© 2019 Published by Elsevier B.V.

Chemical Engineering Journal, Volume 382, February 2020, Article number 122942
DOI:10.1016/j.cej.2019.122942

Experimental study of a single char particle combustion characteristics in a fluidized bed under O_2/H_2O condition

Lin Li[1], Lunbo Duan[1,*], Zhihao Yang[1], Shuai Tong[1], Edward John Anthony[2], Changsui Zhao[1]

1. Key Laboratory of Energy Thermal Conversion and Control of Ministry of Education, School of Energy and Environment, Southeast University, Sipailou 2#, Nnajing, 210096, China

2. Centre for Combustion and CCS, School of Energy, Environment and Agrifood, Cranfield University, Cranfield, Bedfordshire MK43 0AL, UK

*Corresponding author. Fax: +86 25 83790147.

E-mail address: duanlunbo@seu.edu.cn

Abstract

Oxy-steam combustion is a potential new route for oxy-fuel combustion with carbon capture from coal-fired power plants. In the present work, the combustion behavior of single char particles were investigated in a transparent fluidized bed combustor under different operating conditions (i.e., gas atmosphere, oxygen concentration, coal rank, location, fluidization number, particle size, and bed temperature). Both pre-calibrated two-color pyrometry and a flexible thermocouple were used to measure the char particle temperature in the combustion tests. Results indicated that the pore structure of the char generated in H_2O atmosphere was better than that generated in CO_2 and N_2 atmospheres. As expected, with increase of oxygen concentration, the burnout time (t_b) decreased, and the particle temperature (T_p) increased. The sequence of burnout times for different rank coal char particles was: anthracite > bituminous coal > lignite. Interestingly, comparing O_2/CO_2 and O_2/N_2 combustion, a shorter t_b and a lower T_p of char could be achieved simultaneously in O_2/H_2O combustion, regardless of location and oxygen concentration. Furthermore, the increase of fluidization number strengthened the mass and heat transfer between the char and the environment, thereby reducing the t_b and T_p of char. With increasing of particle size, the T_p slightly decreased, the t_b increased markedly, and the gasification reactions became more and more significant. As the bed temperature increased, the gasification rate increased exponentially, and the mass transfer coefficient increased gradually.

Keywords: Fluidized bed; single char particle; O_2/H_2O combustion; particle temperature; burnout time.

Nomenclature

A_0	pre-exponential factor
A_{eff}	effective gasification reaction area of char, m^2
A_p	superficial area of char, m^2
Ar	Archimedes number, dimensionless
a	instrument constant
B	spectral response of blue spectral band for the camera
Bi	Biot number, dimensionless
C_1	first radiation constants, 3.741832×10^8 W·μm^4/m^2
C_2	second radiation constants, 1.438769×10^4 μm·K
C_d	isolated sphere drag coefficient
c_{O2}	difference in oxygen concentration between particle surface and environment, g/m^3
C_p	specific heat capacity, J/kg K
d	diameter, m
v_{gas}	char oxidation rate
Y	mass transfer coefficient, m/s
z	cross-section factor

Greek letters

ε_{mf}	voidage of bed at minimum fluidizing velocity
ε_p	emission rate of particle char
ε_s	emission rate of the surrounding
ε_w	average surface void fraction
ε_r	emission rate of char
ε_λ	spectral emissivity at wavelength λ
λ	wavelength, m
λ_h	heat conductivity coefficient of particle W/(m·K)
μ	dynamic viscosity, N·s/m^2

Published by Elsevier. This is the Author Accepted Manuscript issued with: Creative Commons Attribution Non-Commercial No Derivatives License (CC:BY:NC:ND 4.0).
The final published version (version of record) is available online at DOI:10.1016/j.cej.2019.122942. Please refer to any applicable publisher terms of use.

D_{O2}	diffusion coefficient of oxygen, m^2/s	ρ_p	density of char particle, kg/m^3
E_a	activation energy, kJ/mol	δ	thickness of the thermal gradient layer, m
f	renewal frequency of particle		
G	spectral response of green spectral band for the camera	σ	Stefan-Boltzmann constant, 5.76×10^{-8} W/m^2K^4
H_1	heat release from char oxidation per unit mass, kJ/kg		
H_2	heat release from char gasification per unit mass, kJ/kg	Ψ	dimensionless parameters for isolated sphere
h	heat transfer coefficient, W/m^2K		
h_{total}	heat transfer coefficient between char and its environment, W/m^2K	τ	tortuosity factor
		τ_p	characteristic time for particle, s
$I_{\lambda,T}$	spectral radiation intensity,	*Subscripts*	
$L_{\lambda,T}$	gray level		
m	mass, kg	b	bubble phase
Nu	Nusselt number, dimensionless	cond	conduction
R	spectral response of red spectral band for the camera	conv	convection
Re	Reynolds number, dimensionless	e	emulsion phase
Sc	Schmidt number, dimensionless	f	fluidization
Sh	Sherwood number, dimensionless	mf	minimum fluidization
S_λ	spectral response of the camera sensor	p	particle
T	temperature, K	pc	particle center
t_b	burnout time, s	ps	particle surface
T_{peak}	peak temperature, K	rad	radiation
u	gas velocity, m/s	s	splash zone
v_{oxi}	char gasification rate, g/s		

1 Introduction

Carbon capture and storage (CCS) technology for fossil fuels is regarded as one of the most effective ways to mitigate the impact of greenhouse gases (GHGs) on global climate. Over the last two decades, oxy-fuel combustion has been widely explored, and is considered to be one of the most promising technologies which can be applied in both new-built and retrofit power plants [1]. However, the low efficiency and high operating costs have always been bottlenecks restricting its commercialization [2]. In 2007, a new route of oxy-fuel combustion (oxy-steam combustion) was proposed by CANMET [3], in which steam was used instead of recycled flue gas (RFG) to moderate the high temperature. This avoids the air leakage associated with the RFG system, and significantly reduces energy consumption of the CO_2 purification unit. In addition, it has other advantages, such as the recovery of latent heat of steam, easy operation, reduction of NO_x and SO_x emissions, etc. [4].

As a clean-coal utilization technique, circulating fluidized bed (CFB) combustion technology has many advantages: 1) fuel flexibility (including low calorific value fuel and solid waste); 2) inherent low pollutant (SO_2/NO_x) emissions; 3) flexible boiler load regulation and furnace temperature control, among others. When oxy-steam combustion and CFB technology are combined, the oxy-steam CFB combustion appears to be a potentially competitive process route. Therefore, the combustion mechanism of coal in O_2/H_2O atmosphere is of particular importance and needs to be systematically studied.

However, existing research on oxy-steam combustion mainly focuses on pulverized coal (PC) furnaces [5-12]. These work suggest that the thermodynamic and economic aspects of oxy-steam combustion provide better performance than that of O_2/CO_2 combustion, because the presence of steam can reduce pollutant emission and promote the ignition and char conversion of coal. Fluidized bed combustion differs significantly from pulverized coal combustion in terms of hydrodynamics, reaction kinetics, and heat transfer, but there are very few publications concerning O_2/H_2O fluidized bed combustion. In our previous work [13], the ignition and volatiles combustion behaviors of lignite particles in a fluidized bed under O_2/H_2O atmosphere have been studied, and the results showed that the ignition delay time of lignite particles in

O_2/H_2O atmosphere was slightly longer than that in O_2/N_2 atmosphere. As the oxygen concentration increased, the temperature of the volatiles flame in H_2O atmosphere differed dramatically from that in N_2 atmosphere. It is well known that good char combustion is essential for fluidized bed boilers (the char combustion process accounts for more than 80% of the coal burnout time [14]). However, combustion behavior of char particles in oxy-steam fluidized bed condition is still not fully studied at present.

Scala et al. [15, 16], Bu et al. [17, 18], and Saucedo et al. [19] have studied char particle combustion characteristics in oxy-fuel fluidized bed reactors, either by experiment or simulation, and found that the gasification of char ($C+CO_2=2CO$, +172 kJ/mol) is not negligible, which becomes more significant at high temperature. Roy and Bhattacharya [20] carried out combustion tests for oxy-fuel fluidized bed combustion, and found that the addition of steam increased the char particle temperature relative to the bed temperature, and the carbon conversion rate increased with increasing steam concentration. As mentioned above, as an active medium, the physicochemical properties (heat and mass transfer characteristics and gasification reactivity) of steam are different from that of N_2 and CO_2 in air combustion and conventional oxy-fuel combustion, which has important implications for the char combustion process.

The temperature of char particles is the most important parameter in char combustion process, which not only affects the char conversion rate, but also has an important influence on the agglomeration performance in boiler and the emission characteristic of pollutants (i.e., SO_x, NO_x and particulate matter). The boiler is like a "black box" during the operation of the fluidized bed; the combustion performance of fuel can only be judged by measuring the gas products. The temperature of coal char is difficult to evaluate accurately, although the actual temperature of char particles in the furnace is critical to the design and operation of fluidized bed boilers.

To the best of our knowledge, the combustion behavior of single coal char particles in a fluidized bed under O_2/H_2O atmosphere is still unstudied. Herein, two-color pyrometry and a thin and flexible thermocouple were used to measure the particle temperature during the tests, and the combustion characteristics of single char particles in a "transparent" fluidized bed combustor under different atmospheres were determined. In addition, the physicochemical properties of coal char produced in different atmospheres have also been analyzed.

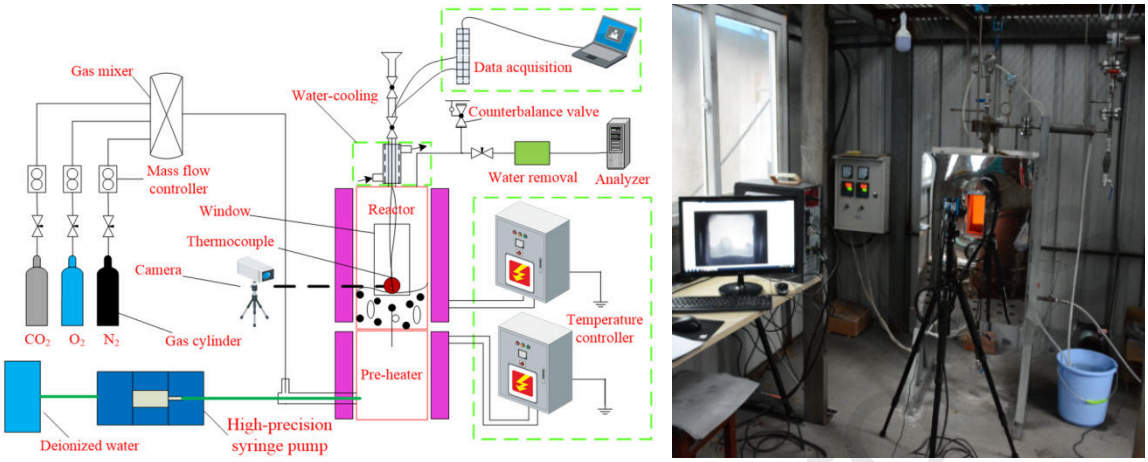
2 Experimental

2.1 Transparent fluidized bed combustor

The tests of the present work were conducted in an electrically heated "optical access" fluidized bed combustor, and the schematic diagram (Fig. 1a) and Photograph (Fig. 1b) of the experimental system are shown in Fig. 1. The test system mainly consists of a gas supply line, a water feeding line, a two-dimensional (length: 200 mm, depth: 34 mm, and height: 400 mm) fluidized bed reactor, a temperature controlling system and a data acquisition system.

The fluidized bed combustor was a two-dimensional reactor with a quartz glass window (height: 200 mm, width: 100 mm, transmittance: >99%) on its front wall, which allows good optical access of the combustion process. O_2, CO_2 and N_2 from cylinders were controlled by digital mass flowmeters, respectively, then fed to the combustor. A high-precision syringe pump was used to control the injection rate of deionized water, and the stream produced after preheating is mixed with O_2 as the fluidization gas. The preheating section and the reactor were heated by two 5 kW electrical heaters, respectively. The bed temperature was measured by a K-type thermocouple which was placed 50 mm above the distributor, and the temperature was continuously controlled by a PID controller within 5 °C deviation during the tests. The detailed description of the experimental system also can be found elsewhere [13, 14]. A color video camera (Nikon D7100) was used to record the char particle combustion process through the window. The concentrations of CO and CO_2 were measured in the reactor outlet with

a gas analyzer (NOVA PLUS, MRU GmbH, German) during the tests, which can be used to assist in determining the burnout time of single char particles, the typical measurement curves of CO_2 and CO are shown in Fig. 2. When the CO concentration is close to zero, the combustion of the char particle can be considered complete.



(a) Schematic diagram of experimental apparatus (b) Photograph of experimental apparatus

Fig. 1. Experimental apparatus.

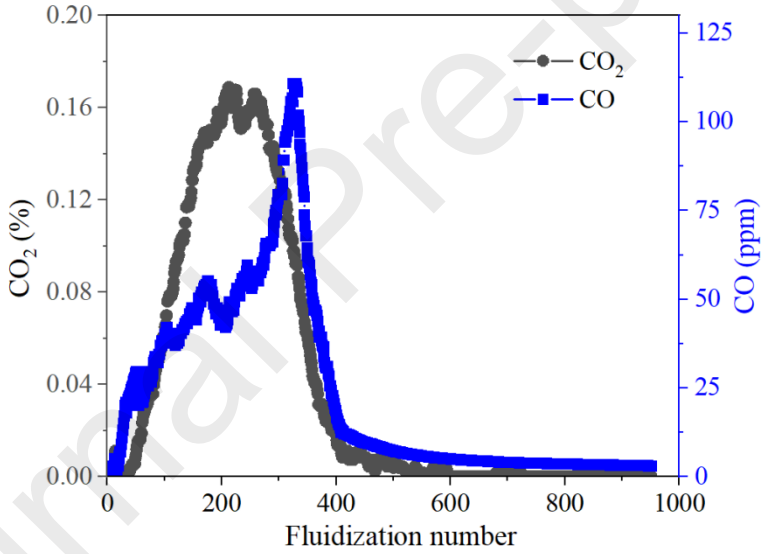


Fig. 2. Typical profiles of the CO_2 and CO concentrations in the exhaust gas during lignite combustion in O_2/N_2 atmosphere, T_b = 800 °C , d_p = 6 mm, u_f/u_{mf} = 3.

2.2 Materials

Three ranks of coal were used as test samples: lignite (LC), bituminous coal (BC) and anthracite (AC). The proximate and ultimate analysis of the coal samples were conducted according to the Chinese standard GB/T212-2008, GB/T214-2007, and GB/T476-2008, as shown in Table 1. In order to avoid the change of char activity due to annealing during char production [21], the in-situ coal char was produced and tested in the present work; i.e., coal particles were used as test samples in the test, rather than coal chars prepared in advance. During the test, when the volatile flame extinguished, the char particle was considered to start burning.

The raw coal particles were first ground into a nearly spherical shape with different diameters (4 mm, 6 mm, 8 mm and 10 mm) before experiment. When the particles were burned in the freeboard, a fine (diam. 0.25 mm) thermocouple was inserted into the coal particle and fixed by sealant to measure the center temperature of the particle. Almost 600 mL of quartz

sand (true density: 2560 kg/m^3) with a particle size range of 0.30-0.35 mm was used as bed material, and the measured minimum fluidization velocity (u_{mf}) was about 0.042 m/s.

Table 1 The proximate and ultimate analysis of the coal samples.

Name		Lignite	Bituminous coal	Anthracite
Proximate analysis, (wt.%, ar)	Moisture	16.17	5.21	1.01
	Volatile	26.29	30.20	8.56
	Fixed carbon	52.45	56.57	78.62
	Ash	5.09	8.02	11.81
Ultimate analysis (wt.%, daf)	Carbon	43.18	81.96	88.22
	Hydrogen	2.72	5.18	4.33
	Oxygen[a]	16.13	11.01	5.68
	Nitrogen	0.93	1.16	1.15
	Sulfur	1.38	0.69	0.62

[a] By difference; ar: as received, daf: dry and ash-free basis.

2.3 Particle temperature measurement

Two-color pyrometry and thermocouples are two kinds of in-situ temperature diagnostic techniques, which were widely used to study fuel particle combustion [6, 13-18, 22]. The thermocouple can accurately measure the particle temperature, but it restricts free movement of the fuel particle in the dense bed, even if the thermocouple is very small [23]. In the present work, when the test was carried out in the dense bed, the particle temperature was only measured by two-color pyrometry. However, in the case of the freeboard, both two-color pyrometry and thermocouple were used.

2.3.1 Two–color pyrometry

The spectral radiation intensity ($I_{\lambda,T}$) is a function of wavelength λ and temperature T, which obeys Planck's radiation law:

$$I_{\lambda,\mathrm{T}} = \varepsilon_\lambda \cdot \frac{C_1}{\lambda^5}\left(e^{\frac{C_2}{\lambda T}} - 1\right)^{-1} \tag{1}$$

where ε_λ is the spectral emissivity at wavelength λ. The wavelengths and temperatures concerned in the present work range from 435.8 to 700 nm and from 1023 to 1573 K, respectively. Since $C_2/\lambda T >> 1$ within these ranges, Planck's law can be replaced by Wien's law:

$$I_{\lambda,\mathrm{T}} = \varepsilon_\lambda \cdot \frac{C_1}{\lambda^5} e^{-C_2/\lambda T} \tag{2}$$

It can be proven that the output of the image, namely the gray level ($L_{\lambda,T}$), is proportional to the radiation intensity of the object and also dependent on the spectral response S_λ of the camera sensor, which can be expressed as:

$$L_{\lambda,\mathrm{T}} = a \cdot S_\lambda \cdot I_{\lambda,\mathrm{T}} = a \cdot S_\lambda \cdot \varepsilon_\lambda \cdot \frac{C_1}{\lambda^5} e^{-C_2/\lambda T} \tag{3}$$

where a is called instrument constant, which is determined by various factors including radiation attenuation, lens properties, observation distance and signal conversion [24]. Applying Eq. (3) to calculate the grey levels at two different wavelengths (λ_1 and λ_2) from the same measurement point, the ratio is given by

$$\frac{L_{\lambda 1,\mathrm{T}}}{L_{\lambda 2,\mathrm{T}}} = \frac{S_{\lambda 1}}{S_{\lambda 2}} \cdot \frac{\varepsilon_{\lambda 1}}{\varepsilon_{\lambda 2}} \cdot \left(\frac{\lambda_2}{\lambda_1}\right)^5 \cdot \exp\left[\frac{C_2}{T} \cdot \left(\frac{1}{\lambda_2} - \frac{1}{\lambda_1}\right)\right] \tag{4}$$

Rearranging Eq. (4), the temperature of the measuring point can be calculated by

Journal Pre-proofs

$$T = \frac{C_2 \cdot [\frac{1}{\lambda_2} - \frac{1}{\lambda_1}]}{\ln \frac{L_{\lambda_1,T}}{L_{\lambda_2,T}} + ln\frac{S_{\lambda_2}}{S_{\lambda_1}} + ln\frac{\varepsilon_{\lambda_2}}{\varepsilon_{\lambda_1}} + \ln(\frac{\lambda_1}{\lambda_2})^5} \quad (5)$$

In Eq. (5), it is crucial to determine the ratio of $\varepsilon_{\lambda 2}$ and $\varepsilon_{\lambda 1}$. Normally, the detected object can be assumed for the grey body, when the used wavelengths are very close to each other, and the size of soot particles in gaseous flames are much smaller than the wavelengths employed [25, 26]. Therefore, the detected object was assumed for the grey body in the present work. The ratio between the spectral sensitivities ($S_{\lambda 2}/S_{\lambda 1}$) is the instrument factor, which can be obtained from the calibration by using a standard temperature source. By defining A as the value of $S_{\lambda 2}/S_{\lambda 1}$ and rearranging Eq. (5), temperature T can be finally resolved as:

$$T = \frac{C_2 \cdot [\frac{1}{\lambda_2} - \frac{1}{\lambda_1}]}{\ln \frac{L_{\lambda_1,T}}{L_{\lambda_2,T}} + lnA + \ln(\frac{\lambda_1}{\lambda_2})^5} \quad (6)$$

2.3.2. Calibration and verification

A blackbody furnace (Landcal R1500T, UK) was used to calibrate the two-color pyrometry. The temperature range is 500-1500 °C with an accuracy of ±1 °C. Before the calibration test, the camera parameters were set to match the experimental situation, including the white balance control, camera aperture, shutter speeds and camera position. In addition, in order to ensure the same light transmittance as in the experiment, an identical quartz glass was fixed in front of the blackbody furnace.

The temperature range of calibration was 800-1300 °C and the temperature interval was 25 °C. Stable temperature was deemed to be achieved when the controller reading was less than ±1 °C. The representative image captured from the blackbody is shown in Fig. 3. Each pixel of image generates three digital numbers (R, G, B), respectively, representing the spectral response of red, green and blue spectral bands for the camera [27]. The central 100×100 pixel from the image was selected to obtain their average value of R, G, and B in order to reduce the effect of noise. According to Eq. (6), the values of ln(R/G) and ln(G/B) for different temperatures are shown in Fig. 4, showing that the red-green two-color has a wider temperature measurement range than that of green-blue. Furthermore, lnA and ln(R/G) have better linearity than that of ln(G/B). Therefore, red and green wavelengths were selected as the measurement temperature band. In order to improve the accuracy of temperature measurement, the formulae were fitted in the range of 1073-1348 K and 1348-1573 K, respectively. The polynomials obtained by fitting the values of lnA and ln(R/G) with R-square of 0.9997 and 0.9912 are shown as follows:
800-1075 °C,

$$\ln A = -0.0105(\frac{R}{G})^4 + 0.1351(\frac{R}{G})^3 - 0.6395(\frac{R}{G})^2 + 0.442(\frac{R}{G}) + 2.3747 \quad (7)$$

1075-1300 °C,

$$\ln A = 59.037(\frac{R}{G})^5 - 96.201(\frac{R}{G})^4 + 59.005(\frac{R}{G})^3 - 16.979(\frac{R}{G})^2 + 1.8731(\frac{R}{G}) + 2.5165 \quad (8)$$

Applying the above equations, it was possible to calculate the temperature distribution of a central 100×100 pixel area of an image obtained at 1125 °C, as shown in Fig. 5. Calculating the average value of these 10000 pixels as the measured temperature, and the comparison between the standard value (black furnace temperature) and measured temperature is presented in Fig. 6. The results indicated that the two series of data are very close, with a maximum difference of 9.02 °C.

Journal Pre-proofs



Fig. 3. Calibration image（4000×6000 pixel）

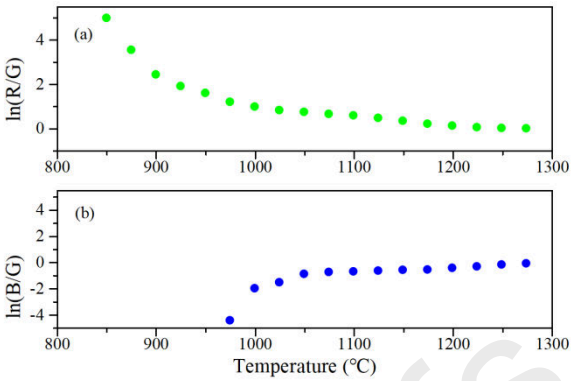


Fig. 4. $\ln^{(L_{\lambda_1,T}/L_{\lambda_2,T})}$

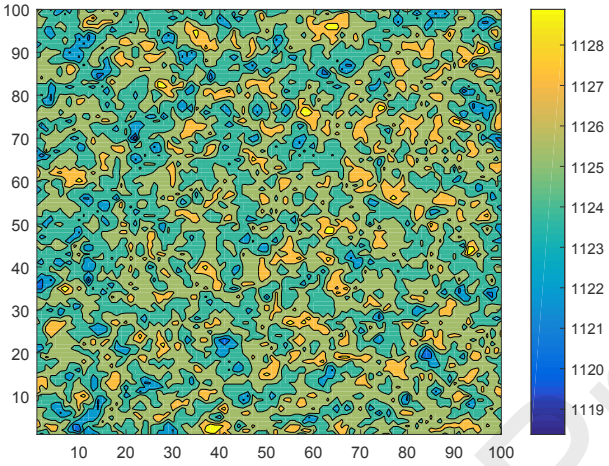


Fig. 5. The temperature measurement result (1125 °C)

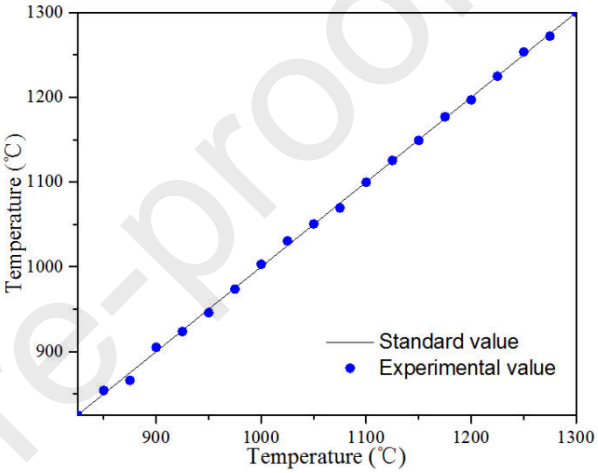


Fig. 6. Comparison of standard and predicted value.

2.4 Experimental procedure

The fluidized bed reactor was heated to target temperature for approximately 3 h and maintained at a constant temperature during the test. The gas velocity (u_f) was set to 2.5-4.5 u_{mf} during the test, which corresponds to vigorous bubbling fluidization conditions. The influence of atmosphere, fuel particle size, bed temperature, fluidization number (u_{f}/u_{mf}) and the effect of coal rank on char combustion behavior were examined in the present work, following the test matrix shown in Table 2. Each condition was repeated more than three times to ensure data reproducibility. Before the tests, a water balance test (ratio of water volume at the outlet of the reactor to the inlet) was performed and the water balance ratio of the experimental system was more than 98% within 2 hours.

Table 2 Test matrix.

Fuel	Atmosphere	O_2 (%)	Location	Bed temperature (°C)	Particle size (mm)	Fluidization number
Lignite, Bituminous coal, Anthracite	O_2/N_2, O_2/CO_2, O_2/H_2O	10, 21, 30, 40	Dense bed, Freeboard	800	6	2.5
Lignite	O_2/N_2, O_2/H_2O	21	Dense bed	750, 850, 900	6	2.5

Journal Pre-proofs

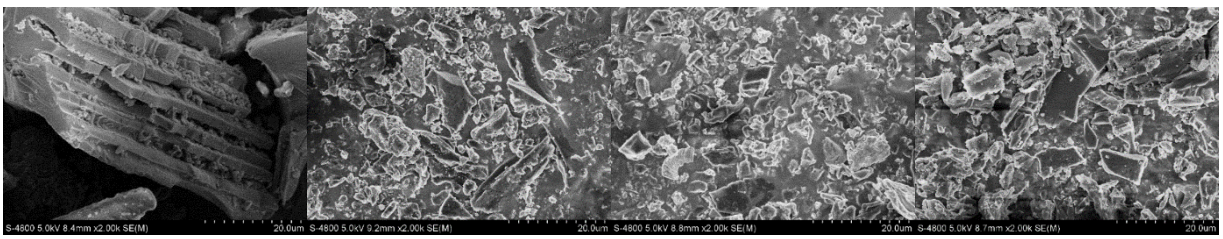
Lignite	O_2/N_2, O_2/H_2O	21	Dense bed	800	4, 8, 10	2.5
Lignite	O_2/N_2, O_2/H_2O	21	Dense bed	800	6	3.5, 4.5

3 Results and discussion

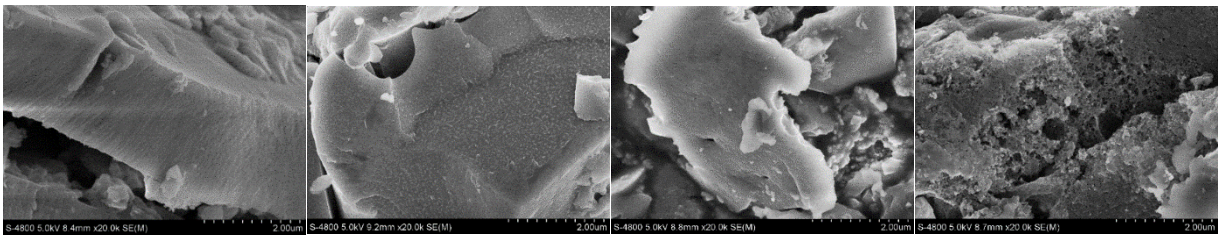
3.1 Physical and chemical properties of char

The char was prepared in a mini-bubbling fluidized bed combustor, because the reactor can be heated and cooled at a faster rate and is easy to operate. The detailed description of the reactor can be found elsewhere [28, 29]. The bed material was quartz sand (size: 0.3-0.35 mm), and the fluidization number was set to 3. The pyrolytic atmospheres were 100% N_2, 100% CO_2 and 50% N_2/50% H_2O, respectively. When the bed temperature was stabilized at 900 °C, coal samples were fed into the reactor; after 7 min, the fluidizing gas was switched to 100% N_2 and the heater was turned off. The char sample was taken out after the bed temperature was brought back to ambient temperature. In addition, the surface morphology of the char was investigated by a Hitachi S-4800 scanning electron microscope (SEM). The pore structure of char was measured by using an accelerated surface area and porosimetry system (Micromeritics ASAP 2020). Specific surface areas and pore size distributions were calculated by the Brunauer–Emmett–Teller (BET) and Barrett–Joyner–Halenda (BJH) methods, respectively.

The SEM images of the original coal and different chars are shown in Fig. 7. It is clear that the original coal sample has a clear layered structure with a smooth surface and very poor pore structure, while the chars (after heat treatment) have more fragmented structures, and the surfaces are rougher and more porous. By directly observing and comparing Fig. 7b, Fig. 7c and Fig. 7d, it can be found that the order of char pore structure produced under different atmospheres is: Char (H_2O) > Char (CO_2) > Char (N_2). In order to quantitatively analyze the pore structure characteristics of different samples, the porosity was measured by N_2 adsorption. The surface area, pore volume and average pore size of different samples are summarized in Table 3. As expected, all char samples showed a larger specific surface area than the coal samples. A large number of pores were formed during the volatiles release process. Here, the specific surface area and pore volume of char produced in H_2O atmosphere was the largest, while that in N_2 atmosphere was the smallest. This indicated that gasification is beneficial to the expansion of the pore structure. Besides, the gasification reactivity of H_2O is faster than that of CO_2, so char pore structure in H_2O atmosphere is greater than that in CO_2 atmosphere. The porous structure of different samples are shown in Fig. 8. In the range of 2-200 nm, the pore structure of chars prepared in N_2 atmosphere is significantly poorer than that of chars prepared in H_2O and CO_2 atmospheres, which is mutually consistent with the results given in Table 1. Interestingly, the porosity of char (CO_2) is around 3 times higher than that of char (H_2O) in the pore size range of 2 – 4 nm, but significantly lower than that of char (H_2O) in the pore size range of 4 – 30 nm, and there is only a small difference in porosity between the char (CO_2) and char (H_2O) in the pore size range of 30 – 200 nm. This means that the char (CO_2) and char (H_2O) have similar macroporous structure, the char (CO_2) has more of a microporous structure, and char (H_2O) has more of a mesoporous structure.



Journal Pre-proofs



(a) Original coal (b) Char (N_2) (c) Char (CO_2) (d) Char (H_2O)

Fig. 7. The SEM images of coal and char samples. (a) Original coal; (b) Char generated in 100% N_2; (c) Char generated in 100% CO_2; (d) Char generated in50% N_2/50% H_2O. The first row of the images were magnified by 2000 and the second row by 20000.

Table 3 Porosity characterization of different samples. (The pyrolysis conditions were 100% N_2, 100% CO_2 and 50%N_2/50%H_2O, respectively, 900 °C, 7 min.)

Sample	Surface area (m^2/g)	Average pore size (nm)	Pore volume (cm^3/g)
Coal	1.9994	2.43	0.0086
Char (N_2)	288.47	2.52	0.0063
Char (CO_2)	483.82	3.47	0.0629
Char (H_2O)	547.77	2.52	0.0914

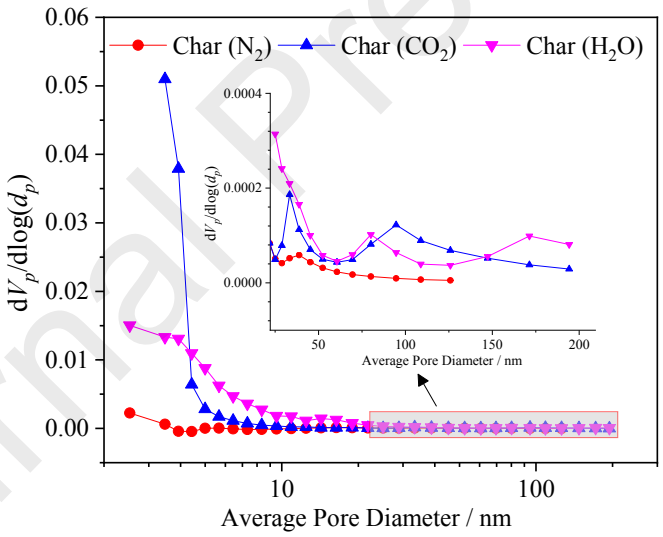


Fig. 8. The pore size distribution of chars from lignite under different atmospheres. The scale of the shaded area between 25 nm and 200 nm is expanded in the insert diagram.

3.2 Overall combustion behavior

The typical temperature curves (including the center and surface temperatures) of a single coal particle combusted in the freeboard are shown in Fig. 9. It should to be pointed out that the char temperature can be measured by two-color pyrometry only when the particles are on the bed surface or in the splash zone, and the sands have little effect on the temperature measurement of char particle. The char combustion process represents the time from when volatiles flame extinguishes to the particles burnout. It is clear that the center temperature of a particle (T_{pc}) and the surface temperature of a particle (T_{ps}) were all significantly higher than bed temperature before the flame extinguished, which can be attributed to heating by the volatiles flame [13]. In addition, in the initial stage of char combustion, the T_{ps} increased rapidly and reached a peak temperature in

Journal Pre-proofs

less than 80 s, and then began to slowly decrease until burnout. Whereas, the T_{pc} slowly increased after a short drop after losing the heating contribution of the volatiles flame, and the peak temperature did not occur until the later stage of char combustion. Interestingly, the peak temperature of T_{pc} and T_{ps} were very close, although appear at different times. Fig. 9 also shown that the peak temperature of T_{ps} (1092.9 °C) was higher than that of T_{pc} (1081.5 °C) in 20% O_2/80% CO_2 atmosphere. This was caused by two reasons: 1) in the initial stage of char combustion, there may be a luminous volatile flame around the char particle, which can improve the char oxidation rate and surface temperature; 2) unlike the intense burning of char surface, the burning of char core was relatively mild due to low oxygen diffusion into the char center, so the peak temperature of T_{pc} was lower than T_{ps}.

Although the peak temperature of T_{pc} and T_{ps} were relatively close, they appear at different time. The difference between the two temperatures was more than 100 °C for a long time, which is because there is a significant temperature gradient along the radius inside the large particle when the particle burning in the dilute phase. In the initial stage of char combustion, the oxidation rate of char surface is more intense than that of char center due to the better oxygen transportation, thus the temperature difference is very significant. In the later stage of char combustion, the surface temperature of particle (ash layer) is already close to the surrounding temperature, while the unburned char in the center of particle is still burning, so the temperature difference between particle center and surface is still large. The temperature gradient of ash shell can be neglected when the char particle burning in dense phase, because the vigorous action of the fluidized bed material removed the ash by attrition from the char surface. Otherwise, as shown in Fig. 9, the char burnout time judged by T_{ps} was underestimated compared to the burnout time obtained from T_{pc}. In this case, the char burnout time was obtained from the flue gas concentration (CO and CO_2).

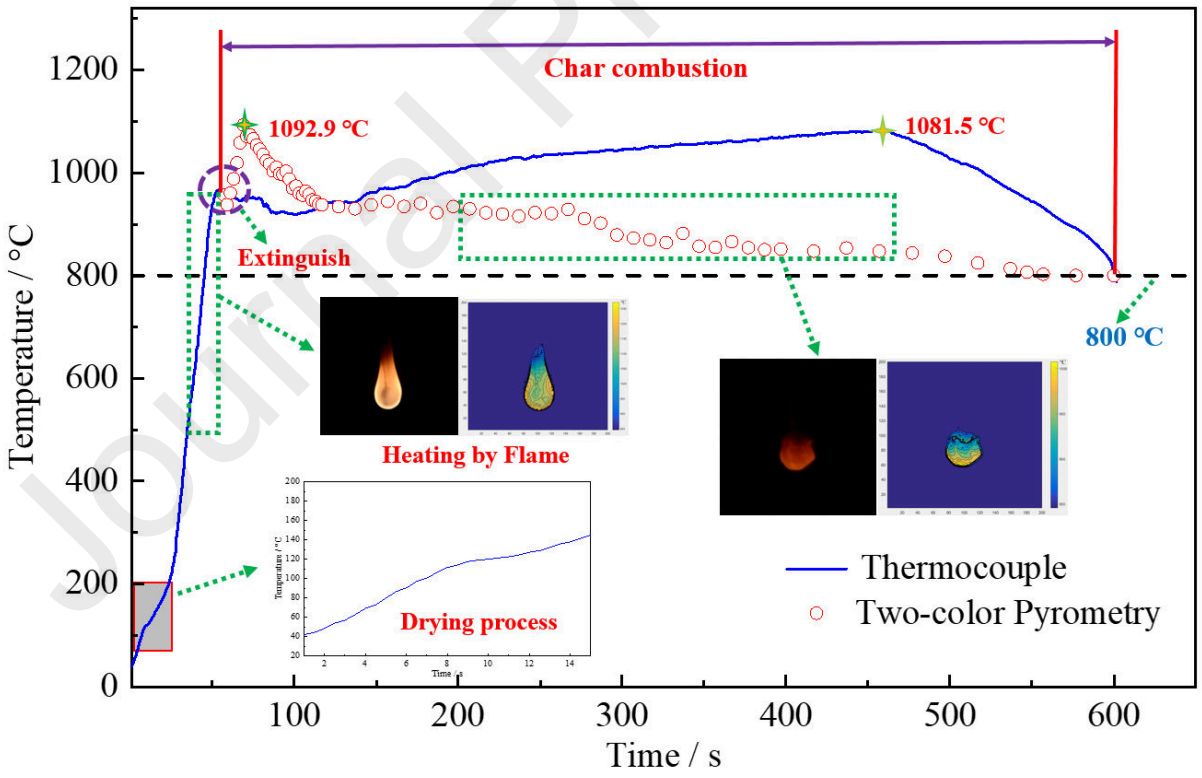


Fig. 9. The typical temperature history of particle center (measured by thermocouple, T_{pc}) and particle surface (measured by two-color pyrometry, T_{ps}) in the dilute phase. d_p = 6 mm, T_b = 800°C, 20%O_2/80% N_2 atmosphere, u_f / u_{mf} = 2.5.

3.3 Effect of atmosphere and fuel type

For a direct comparison, the peak temperatures of char (T_{peak}) under different conditions are plotted in Fig. 10. It is obvious that under the same operating conditions, the T_{peak} of bituminous coal was slightly higher than that of anthracite and lignite, but the temperature difference between them was less than 50 °C. In the freeboard, the T_{peak} was obviously higher than that in the dense bed, which is attributed to the higher mass transfer coefficient in the freeboard [14]. As expected, the T_{peak} increased with the oxygen concentration. At the same operating conditions, the T_{peak} sequence was: O_2/N_2>O_2/H_2O>O_2/CO_2, and this can be explained by the thermal equilibrium equation for char particles:

$$c_p m \frac{dT_p}{dt} = H_1 \cdot v_{oxi} + H_2 \cdot v_{gas} - q_{total} = H_1 \cdot \pi d_p \cdot ShD_{o_2} \cdot c_{O2} + H_2 \cdot A_{eff} \cdot A_0 \cdot exp\left(-\frac{E_a}{RT_p}\right) - h_{total} \cdot A_p \quad (9)$$

It should be pointed out that the Biot number of char in dense phase and freeboard was close to 0.1 (at 800°C, d_p = 6 mm, 0.158 and 0.108, respectively), thus, the particle temperature may be considered to be approximately uniform. Herein, the gasification endothermic reaction between gasification agent (H_2O or CO_2) and char will reduce the particle temperature in oxy-fuel combustion, and the effect of gasification is more significant at high oxygen concentrations due to the high particle temperature [29, 30]. Also, the specific heat capacities of CO_2 and H_2O are higher than that of N_2, which is supposed to bring a higher thermal convection in h_{total}. Finally, the oxidation of char in a fluidized bed can be considered as external diffusion control [15, 18, 20, 31]. At 800 °C, the D_{O2} in N_2, H_2O and CO_2 are 1.96 cm^2/s, 2.51 cm^2/s and 1.59 cm^2/s, respectively, and the higher D_{O2} means greater v_{oxi} and T_p.

The burnout times of char (t_b) in different atmospheres and fuel types are summarized in Fig. 11. It is clear that the order of t_b for different fuel types is: anthracite > bituminous coal > lignite, mainly attributed to the high rank coal with high fixed carbon content (see Table 1) and low reactivity of char. It is generally believed that a higher oxygen concentration produces a higher particle temperature and a lower burnout time, while a high T_p corresponds to a low burnout time at the same oxygen concentration [14, 17]. However, surprisingly, it can be seen from Fig. 10 and Fig. 11 that the char particle has both lower temperature and burnout time in O_2/H_2O atmosphere, which may be beneficial in reducing pollutant emissions and reducing bed agglomeration. This was caused by a combination of several factors: 1) diffusion. A higher oxygen diffusion leads to a shorter burnout time and a higher char temperature; 2) gasification. Although gasification is an endothermal reaction and thus will reduce the char temperature, it increases the carbon conversion rate and reduces burnout time; 3) competition between gasification and oxidation. There is a competitive relationship between oxidation and gasification of char, and the strength of the competition may be related to bed temperature, oxygen concentration and fuel type, etc. [29, 32]. Otherwise, interestingly, as the oxygen concentration increases, the T_p in O_2/H_2O combustion increased more significantly than that in other atmospheres. This may be attributed to the higher D_{O2} in O_2/H_2O atmosphere. Similar phenomena were also observed by Zou et al. [6], who carried out pulverized coal combustion in a drop tube furnace. In addition, as shown in Table 3, the char produced in H_2O atmosphere has a larger pore structure and specific surface area than that produced in N_2 and CO_2 atmospheres, which not only is conducive to the oxygen internal diffusion of char particle, but also greatly improves the effective reactive area of char. So the participation of H_2O in the combustion process reduces the particle temperature and increases the char conversion rate by increasing the $D_{O2,}$ pore structure of char and gasification. This unique behavior provides a guide for bed temperature control when operating oxy-fuel fluidized bed boilers at high oxygen concentration.

Journal Pre-proofs

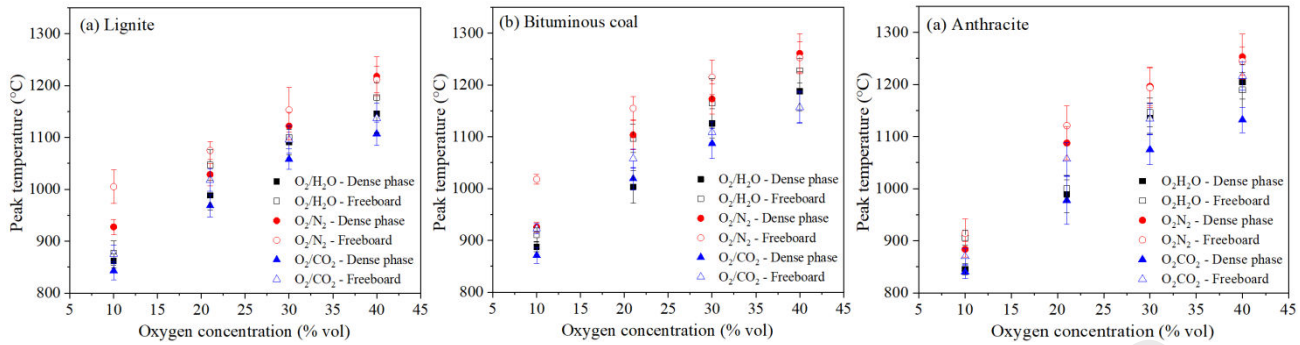


Fig. 10. The peak temperature of coal particles in various O_2 concentrations under N_2 and CO_2 atmosphere. d_p = 6 mm, T_b = 800°C, u_f / u_{mf} = 2.5. (The burnout time in O_2/N_2 and O_2/CO_2 atmospheres with 10% and 30% oxygen are from previous studies [11].)

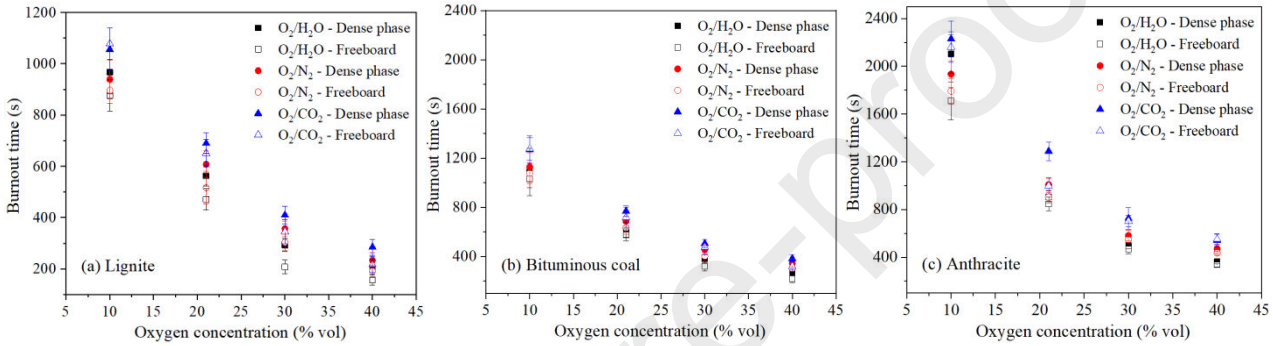


Fig. 11. The burnout time of coal particles in various O_2 concentrations under N_2 and CO_2 atmosphere. d_p = 6 mm, T_b = 800°C, u_f / u_{mf} = 2.5. (The peak temperature in O_2/N_2 and O_2/CO_2 atmospheres with 10% and 30% oxygen are from previous studies [11].)

3.4 Effect of fluidization number (u_f / u_{mf})

The variation of char temperature and burnout time vs. fluidization number are shown in Fig. 12. It is clear that both the temperature and the burnout time decreased with the increase of fluidization number, in spite of the nature of the atmosphere. The higher fluidization number results in a larger bubble size and higher bubble frequency [33], which will significantly increase the probability of char particles spending time in the splash zone and bubble phase [34]. Otherwise, the mass transfer coefficient (Y_{O2}) of O_2 in the freeboard and splash zone also increased with fluidization number (as shown in Table 4; the detailed calculation for the process can be seen in Appendix A), thus the t_b reduced as w increased. When the fluidization number increased from 2.5 to 4.5, the t_b in O_2/H_2O and O_2/N_2 atmospheres decreased by 30.14% and 21.22%, respectively. Compared to O_2/N_2 combustion, the higher reduction of t_b in O_2/H_2O atmosphere was caused by its higher D_{O2}. Fig. 12 also shows that the T_{peak} decreased as the fluidization number increased, which may be attributed to the increase of the heat transfer coefficient (h_{total}) between the char particle and atmosphere at high fluidization number. The value for h_{total} can be calculated by

$$h_{total} = h_{cond} + h_{conv} + h_{radi} \quad (10)$$

Here h_{cond} represents the heat conduction between char and bed material; and h_{conv} and h_{radi} are the heat of convection and the radiation between char and environment, respectively. The heat transfer coefficients under different operating conditions are shown in Table 4. The detailed calculation process is given in Appendix B. It should be noted that if the fluidization number continues to increase, the char temperature will continue to decrease until it is close to the bed temperature. In this case, the char oxidation reaction will gradually move from the diffusion control to the kinetic control due to the decrease of particle

temperature, so the increase of mass transfer coefficient will have less and less influence on the t_b of char.

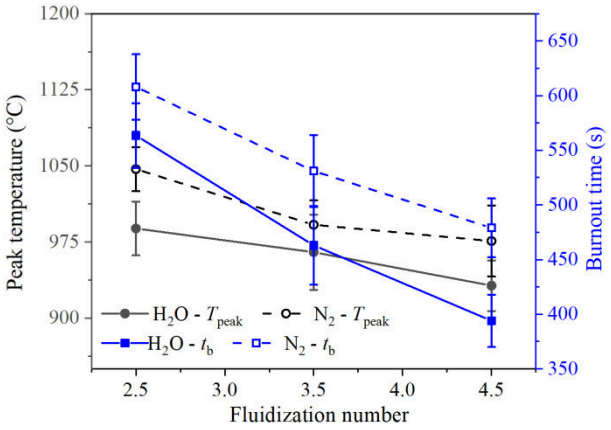


Fig. 12. The variation of char temperature and burnout time vs. fluidization number. (d_p = 6 mm, 21% O_2, T_b = 800 °C, lignite).

Table 4 The variation of relevant parameters vs. fluidization number. (d_p = 6 mm, 21% O_2, T_b = 800°C, lignite)

u_f / u_{mf}	Heat transfer coefficient (W/m²K)				Mass transfer coefficient (m/s)		
	h_{cond}	$h_{conv,\ dense}$	$h_{conv,\ freeboard}$	h_{radi}	$Y_{O2,\ e}$	$Y_{O2,\ b}$	$Y_{O2,\ s}$
2.5	132.33	6.42	44.81	78.15	0.051	0.09	0.11
3.5	145.61	6.45	47.88	75.72	0.051	0.10	0.12
4.5	156.39	6.48	50.55	72.40	0.051	0.11	0.13

3.5 Effect of particle size

The variation of T_{peak} and t_b vs. particle diameter under O_2/N_2 and O_2/H_2O atmospheres at 800 °C, is plotted in Fig. 13. It is clearly shown that the t_b was significantly increased with the increase of d_p in both O_2/N_2 and O_2/H_2O atmospheres, which is to be expected. Fig. 14 shows the variation of Biot number (Bi) and d_p^2 vs. particle size. It can be found that the char combustion in O_2/N_2 atmospheres followed the classical t_b - d_p^2 law (Nusselt square law), which can be expressed as:

$$t_b = 11.68\ d_p^2 + 170.24,\ R^2 = 0.992 \tag{11}$$

This supports the contention that the char particle combustion in O_2/N_2 atmosphere is controlled by mass diffusion in the boundary layer [35, 36]. However, the char combustion in O_2/H_2O atmosphere did not follow the Nusselt square law, especially for large particles. This is also evident given that char gasification has a non-negligible effect in O_2/H_2O combustion. A similar conclusion was also obtained by Wang et al. [30], who studied the burnout time of char in O_2/CO_2 and O_2/N_2 atmospheres. Fig. 13 also shows that the T_{peak} slightly decreased as the d_p increased. Rearranging Eq. (10), T_p can be evaluated by

$$\frac{dT_p}{dt} = 6[H_1 \cdot \frac{ShD_{O2}}{d_p} \cdot c_{O2} + H_2 \cdot A_0 \cdot exp\left(-\frac{E_a}{RT_p}\right) - h_{total}] / (c_p \cdot d_p \cdot \rho_p) \tag{12}$$

Obviously, the particle temperature is inversely proportional to the value of d_p. It must also be pointed out that Eq. (11) can only be used for qualitative analysis because herein the assumption is that the particle temperature is uniform, which is difficult to achieve in the large char particle combustion process. As shown in Fig. 14, when the d_p = 4 mm, Bi = 0.104, the particle temperature can be approximated as being uniform ($Bi \approx 0.1$), and when the d_p is larger than 4 mm, $Bi > 0.1$, the temperature gradient inside the particle will gradually increase, the difference between T_{pc} and T_{ps} will also increase as the particle size increases.

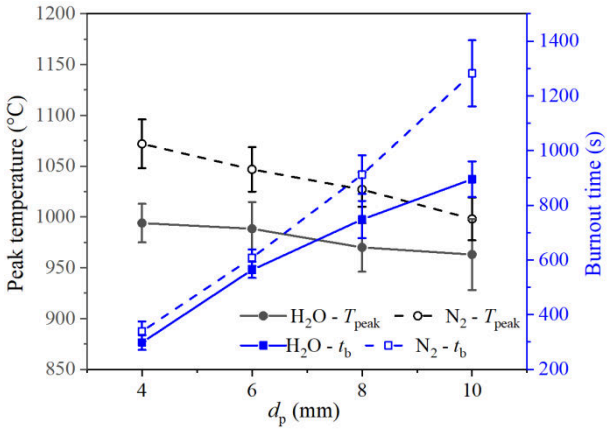


Fig. 13. The variation of char temperature and burnout time vs. particle size. (u_f/u_{mf} = 2.5, 21% O_2, T_b = 800 °C, lignite)

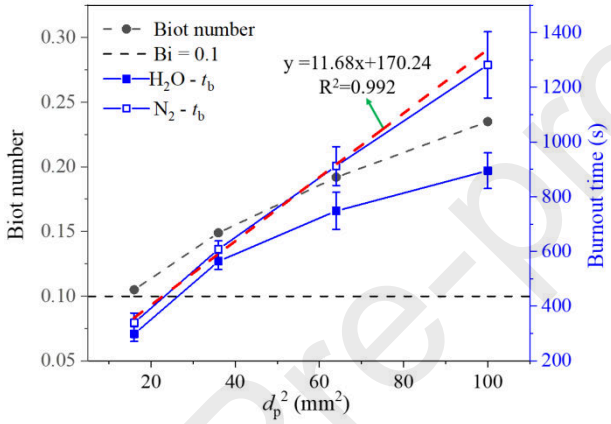


Fig. 14. The variation of relevant parameters vs. particle size. (u_f/u_{mf} = 2.5, 21% O_2, T_b = 800 °C, lignite)

3.6 Effect of bed temperature

The variation of char temperature and burnout time vs. bed temperature is shown in Fig. 15. As expected, as the bed temperature increases, the T_{peak} of char particle increased and the corresponding burnout time decreased in both O_2/N_2 and O_2/H_2O atmospheres. This was mainly because the D_{O2} increases with increasing temperature, and the oxidation rate of char will be accelerated at high temperature. Surprisingly, it was found that the reduction of t_b in O_2/H_2O atmosphere was more pronounced than that in N_2 atmosphere. As shown in Fig. 16, the value of $t_{b,N2}$ / $t_{b,H2O}$ increased from 1.02 at a bed temperature of 750 °C to 1.3 at 900 °C. This appears to be related to two factors: 1) the diffusion rate of oxygen (the value of $D_{O2/H2O}/D_{O2/N2}$ is 1.28, which remains constant as the temperature increases; higher D_{O2} means more char oxidation); and 2) enhanced gasification in H_2O atmosphere. As the temperature rises, the gasification rate shows almost exponential growth, which benefits char consumption, although the gasification will itself reduce the particle temperature.

Fig. 16 also shows that the mass transfer coefficient ($v_{gas,\ H2O}$) of oxygen in O_2/H_2O atmosphere was much greater than that in O_2/N_2 atmosphere ($v_{gas,\ N2}$), and the gap becomes greater as the temperature increases. Furthermore, the value of $D_{O2/H2O}/D_{O2/CO2}$ is 1.62, so the O_2/H_2O combustion is more advantageous than O_2/CO_2 combustion.

Journal Pre-proofs

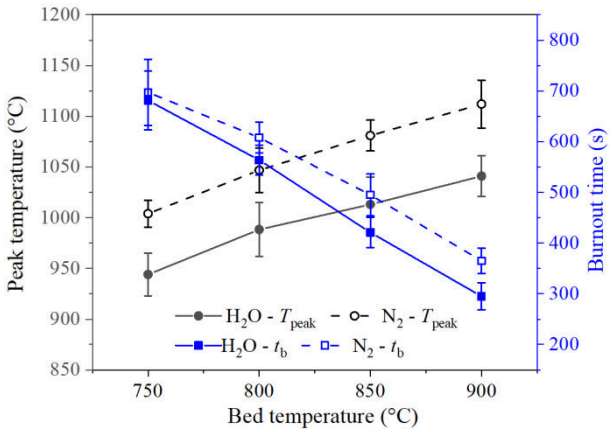


Fig. 15. The variation of char temperature and burnout time vs. bed temperature. (u_f / u_{mf} = 2.5, 21% O_2, d_p = 6 mm, lignite)

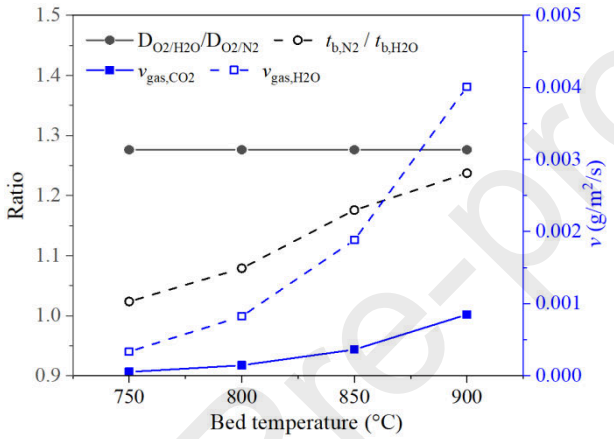


Fig. 16. The variation of related parameters vs. temperature. (u_f / u_{mf} = 2.5, 21% O_2, d_p = 6 mm, lignite)

4. Conclusions

The present work employed two-color pyrometry and thermocouples to monitor the temperature of particles in experimental studies of combustion behavior of single char particles in a transparent fluidized bed reactor. Different coal rank, atmosphere (O_2/H_2O, O_2/N_2 and O_2/CO_2), oxygen concentration (10% - 40%), location (dense bed and freeboard), fluidization number (2.5, 3.5, 4.5), particle size (4, 6, 8, 10 mm) and bed temperature (750 - 900 °C) were employed and the major conclusions are summarized below.

(1) The gasification reaction of CO_2 and H_2O with coal char can increase the pore structure of coal char, and H_2O-char gasification is significantly greater than that of CO_2-char; thus the order of char pore structure produced under different atmospheres is: Char (H_2O) > Char (CO_2) > Char (N_2);

(2) Due to the higher D_{O2} and the char gasification rate in O_2/H_2O atmosphere, the char had the shortest burnout time and a relatively low particle temperature in O_2/H_2O combustion compared to the O_2/N_2 and O_2/CO_2 combustion;

(3) Under the same atmosphere, the char burned in the freeboard had shorter burnout time and higher particle temperature than that in the dense bed, and the burnout time sequence of coal char was: anthracite > bituminous coal > lignite;

(4) Compared to conventional O_2/N_2 and O_2/CO_2 combustion, O_2/H_2O combustion is better for operation under high oxygen concentration and high bed temperature, because both gasification and oxidation are significantly enhanced, which not only results in higher carbon conversion rates, but also ensures a relatively low particle temperature, which is beneficial in reducing pollutant emissions and reducing bed agglomeration;

(5) With the increase of fluidization number, both the mass and heat transfer between gas environment and char were

enhanced, so lower particle temperature and shorter burnout time could be obtained simultaneously.

Acknowledgment

This work was financially supported by the National Natural Science Foundation of China (51776039), Scientific Research Foundation of Graduate School of Southeast University, China (YBJJ1852), and the Program of China Scholarships Council (NO. 201806090039).

Appendix A. The Calculation of mass transfer coefficient (*h*)

The mass transfer coefficient of oxygen (Y_{O2}) can be caculated by:

$$Y_{O2} = \frac{Sh \cdot D_{O2}}{d_p} \tag{A1}$$

When the char particle was burned in dense phase, it may move into the emulsion, bubble and splash areas. The *Sh* can be expressed [37, 38]:

In the emulsion phase, $$Sh_e = \frac{2\varepsilon_{mf}}{\tau} + 0.3465(Re_e C_{d,e})^{0.33}\left(\frac{\tau}{\varepsilon_{mf}}\right)^{0.66}((1 + Re_e Sc)^{0.33} - 1)$$ (A2)

In the bubble phase, $$Sh_b = 2 + 0.3465(Re_b C_{d,b})^{0.33}((1 + Re_b Sc)^{0.33} - 1)$$ (A3)

In the splash zone, $$Sh_s = 2 + 0.69(Re_s)^{0.5} Sc^{0.33}$$ (A4)

In the present work, $\varepsilon_{mf} = 0.45$. The calculation of relevant parameters in Eq. (A2)-(A4) are shown in Table A1.

Table A1 The calculation for relevant parameters.

Parameter	Nomenclature	The formula for relevant parameters	Reference
Re	Reynolds number	$Re_e = \rho \cdot u_{mf} \cdot d_p/\mu$, $Re_b = Re_s = \rho \cdot u_f \cdot d_p/\mu$	-
Sc	Schmidt number	$Sc = \mu/(\rho \cdot D_{O2})$	-
C_d	Isolated sphere drag coefficient	$C_{d,e} = \frac{24}{Re_e}\left(\frac{2z(1-\varepsilon_{mf})}{\tau}\right) + (10^{\Psi_e} - 1)$, $C_{d,b} = \frac{24}{Re_b}10^{\Psi_b}$	[39], [40]
z	Cross-section factor	$z = \frac{5.3}{\tau^2}\left(\frac{\varepsilon_{mf}}{1-\varepsilon_{mf}}\right)^{0.33}$	[41]
τ	Tortuosity	$\tau = [1 - 0.9(\varepsilon_{mf} - 0.25)^{1/3}(1 - \varepsilon_{mf})^{2/3}]^{-1}$	[39]
Ψ	Dimensionless parameters	$\Psi = 0.261Re^{0.369} - 0.105Re^{0.431} - \frac{0.124}{1 + (\log_{10}Re)^2}$	[40]

Appendix B. The Calculation of heat transfer coefficient

The heat transfer coefficient of oxygen (*h*) can be caculated by:

$$h_{total} = h_{cond} + h_{conv} + h_{radi} \tag{B1}$$

The h_{cond} can be calculated by [42]:

$$h_{cond} = \rho_p \cdot c_p \cdot \delta \cdot (1 - \varepsilon_w) \cdot \frac{f}{1 + f \cdot \tau_p} \tag{B2}$$

The detailed calculated of revelant parameters can be found in reference [42, 43]. The h_{conv} can be expressed [42]:

Journal Pre-proofs

$$h_{conv} = (1 - \varepsilon_b)h_{mf} + \varepsilon_b h_b = (1 - \varepsilon_b) \times 0.86Ar^{0.39}\frac{\lambda_h}{d_p^{0.5}} + \varepsilon_b \times 0.0175Ar^{0.46}Pr^{0.33}(\frac{u}{u_{mf}})^{0.3}\frac{\lambda_h}{d_p} \quad (B3)$$

h_{mf} is the heat transfer coefficient at minimum fluidization velocity; can be estimated by the method of Botterill et al. [44]; δ_b is the bubble fraction within the fluidized bed, which can be calculated by the classical two-phase theory for aggregative fluidization [45]. The contribution to heat transfer coefficient due to the rising bubbles, h_b, is calculated by [46]. The h_{radi} can be calculated by [42, 47, 48]:

$$h_{radi} = \frac{\sigma (T_p - T_b) \cdot (T_p^2 + T_b^2)}{(\frac{1}{\varepsilon_p} + \frac{1}{\varepsilon_w} - 1)} \quad (B4)$$

In the present work, ε_p= 0.85, ε_w = 0.25.

References

[1] B. J. Buhre, L. K. Elliott, C. D. Sheng, R. P. Gupta, T. F. Wall, Oxy-fuel combustion technology for coal-fired power generation, Prog. Energy Combust. Sci. 31 (4) (2005) 283-307.

[2] M. B. Toftegaard, J. Brix, P. A. Jensen, P. Glarborg, A. D. Jensen, Oxy-fuel combustion of solid fuels, Prog. Energy Combust. Sci. 36 (5) (2010) 581-625.

[3] C. Salvador, Modeling design and pilot-scale experiments of CANMET's advanced oxy-fuel/steam burner, 25 International oxy-combustion research network 2nd workshop, Windsor, USA, 2007, p. 26

[4] S. Seepana, S. Jayanti, Steam-moderated oxy-fuel combustion, Energy Convers. Manage. 51 (10) (2010) 1981–1988.

[5] C. Zou, L. Cai, D. Wu, Y. Liu, S. Liu, C. Zheng, Ignition behaviors of pulverized coal particles in O_2/N_2, and O_2/H_2O mixtures in a drop tube furnace using flame monitoring techniques, Proc. Combust. Inst. 35 (3) (2015) 3629-3636.

[6] S. Lei, X. Liu, J. Si, Y. Xu, Z. Zhou, and M. Xu, Simulation and comparative exergy analyses of oxy-steam combustion and O_2/CO_2 recycled combustion pulverized-coal-fired power plants, Int. J. Greenh. Gas Con. 27 (8) (2014) 267-278.

[7] B. Jin, H. Zhao, C. Zou, C. Zheng, Comprehensive investigation of process characteristics for oxy-steam combustion power plants, Energy Convers. Manag. 99 (2015): 92-101.

[8] C. Zou, L. Zhang, S. Cao, C. Zheng, A study of combustion characteristics of pulverized coal in O_2/H_2O atmosphere, Fuel 115 (2014) 312-320.

[9] G. A. Richards, K. H. Casleton, B. T. Chorpening, CO_2 and H_2O diluted oxy-fuel combustion for zero-emission power, P. I. Mech. Eng. A-J. Pow. 219 (2) (2005) 121-126.

[10] K. Lei, B. Ye, J. Cao, R. Zhang, D. Liu, Combustion characteristics of single particles from bituminous coal and pine sawdust in O_2/N_2, O_2/CO_2, and O_2/H_2O atmospheres. Energies 10 (11) (2017) 1695-1706.

[11] L. Zhang, C. Zou, D. Wu, Y. Liu, C. Zheng, A study of coal chars combustion in O_2/H_2O mixtures by thermogravimetric analysis, Journal of Thermal Analysis and Calorimetry, 126 (2) (2016) 995-1005.

[12] B. Ye, R. Zhang, J. Cao, K. Lei, D. Liu, The study of co-combustion characteristics of coal and microalgae by single particle combustion and TGA methods. Journal of the Energy Institute, (2019) https://doi.org/10.1016/j.joei.2019.07.001.

[13] L. Li, L. Duan, D. Zeng, D.Y. Lu, C, Zhao, Ignition and volatiles combustion behaviors of a single lignite particle in a fluidized bed under O_2/H_2O condition, Proc. Combust. Inst. 37 (4) (2019) 4451-4459.

[14] L. Duan, L. Li, D. Liu, C, Zhao, Fundamental study on fuel-staged oxy-fuel fluidized bed combustion, Combust. Flame 206 (2019) 227-238.

Journal Pre-proofs

[15] F. Scala, R. Chirone, Combustion of Single Coal Char Particles under Fluidized Bed Oxyfiring Conditions, Ind. Eng. Chem. Res. 49 (2009) 11029-11036.

[16] F. Scala, R. Chirone, Fluidized bed combustion of single coal char particles at high CO_2 concentration, Chem. Eng. J. 165 (3) (2010) 902-906.

[17] C. Bu, D. Pallarès, X. Chen, A. Gómez-Barea, D. Liu, B. Leckner, P. Lu, Oxy-fuel combustion of a single fuel particle in a fluidized bed: char combustion characteristics, an experimental study, Chem. Eng. J. 287 (2016) 649-656.

[18] C. Bu, A. Gómez-Barea, X. Chen, B. Leckner, D. Liu, D. Pallarès, P. Lu, Effect of CO_2, on oxy-fuel combustion of coal-char particles in a fluidized bed: Modeling and comparison with the conventional mode of combustion, Appl. Energy 177 (2016) 247-259.

[19] M. A. Saucedo, M. Butel, S. A. Scott, N. Collings, J. S. Dennis, Significance of gasification during oxy-fuel combustion of a lignite char in a fluidized bed using a fast UEGO sensor, Fuel 144 (15) (2015) 423-438.

[20] B. Roy, S. Bhattacharya, Combustion of single char particles from Victorian brown coal under oxy-fuel fluidized bed conditions. Fuel 165 (2016) 477-483.

[21] C. Chen, J. Wang, W. Liu, S. Zhang, J. Yin, G. Luo, H. Yao, Effect of pyrolysis conditions on the char gasification with mixtures of CO_2 and H_2O, Proc. Combust. Inst. 34 (2) (2013) 2453-2460.

[22] J. S. Chern, A. N. Hayhurst, Fluidised bed studies of: (i) Reaction-fronts inside a coal particle during its pyrolysis or devolatilisation, (ii) the combustion of carbon in various coal chars, Combust. Flame 159 (2012) 367-375.

[23] J. Salinero, A. Gómez-Barea, D. Fuentes-Cano, B. Leckner, The effect of using thermocouples on the char particle combustion in a fluidized bed reactor, Fuel 207 (2017) 615-624.

[24] D. Liu, J. Yan, F. Wang, Q. Huang, Y. Chi, K. Cen, Experimental reconstructions of flame temperature distributions in laboratory-scale and large-scale pulverized-coal fired furnaces by inverse radiation analysis, Fuel 93 (2012) 397-403.

[25] T. S. Draper, D. Zeltner, D. R. Tree, Y. Xue, R. Tsiava, Two-dimensional flame temperature and emissivity measurements of pulverized oxy-coal flames, Appl. Energy 95 (2012) 38-44.

[26] J. M. Char, W. J. Liou, J. H. Yeh, C. L. Chiu, Ignition and combustion study of JP-8 fuel in a supersonic flowfield, Shock Waves 6 (1996) 259-266.

[27] Y. Huang, Y. Yan, Transient two-dimensional temperature measurement of open flames by dual-spectral image analysis, T. I. Meas. Control 22 (5) 2000 371-384.

[28] S. Tong, L. Li, L. Duan, C. Zhao, E. J. Anthony, A kinetic study on lignite char gasification with CO_2 and H_2O in a fluidized bed reactor, Appl. Therm. Eng. 147 (2019) 602-609.

[29] L. Li, L. Duan, S. Tong, E. J. Anthony. Combustion characteristics of lignite char in a fluidized bed under O_2/N_2, O_2/CO_2 and O_2/H_2O atmospheres, Fuel process. Tech., 186 (2019) 8-17.

[30] W. Wang, C. Bu, A. Gómez–Barea, B. Leckner, X. Wang, J. Zhang, G. Piao, O_2/CO_2 and O_2/N_2 combustion of bituminous char particles in a bubbling fluidized bed under simulated combustor conditions, Chem. Eng. J. 336 (2018) 74-81.

[31] J. Salinero, A. Gómez-Barea, D. Fuentes-Cano, B. Leckner, Measurement and theoretical prediction of char temperature oscillation during fluidized bed combustion, Combust. Flame 192 (2018) 190-204.

[32] O. Senneca, L. Cortese, Kinetics of coal oxy-combustion by means of different experimental techniques, Fuel 102 (2012) 751-759.

Journal Pre-proofs

[33] L. Li, Y. Duan, L. Duan, C. Xu, E.J. Anthony, Flow characteristics in pressurized oxy-fuel fluidized bed under hot condition, Int. J. Multiphas. Flow 108 (2018), 1-10.

[34] Z. Yang, L. Duan, L. Li, D. Liu, Movement and mixing of biomass or coal particles in a fluidized bed combustor under high temperatures [C], Fluidization XVI, May, 2019, Guilin, China.

[35] M. A. Andrei, A. F. Sarofim, J. M. Beer, Time-resolved burnout of coal particles in a fluidized bed, Combust. Flame 61 (1) (1985) 17–27.

[36] M. Zhu, Z. Zhang, Y. Zhang, H. X. Setyawan, P. Liu, D. Zhang, An experimental study of the ignition and combustion characteristics of single droplets of biochar-glycerol-water slurry fuels, Proc. Combust. Inst. 36 (2) (2017) 2475-2482.

[37] M. J. Biggs, P. K. Agarwal, Mathematical modelling of oscillations in the temperature of freely moving burning carbonaceous particles in bubbling fluidized beds, Fuel 72 (1993) 805-811.

[38] P. N. Rowe, K. T. Claxon, J. B. Lewis, Heat and mass transfer from a single sphere in an extensive flowing fluid, Trans. Inst. Chem. Eng. 43 (1965) 14-31.

[39] P. K. Agarwal, B. K. O'Neill, Transport phenomena in multi-particle systems-I. Pressure drop and friction factors: Unifying the hydraulic-radius and submerged-object approaches, Chem. Eng. Sci. 43 (1988) 2487-2499.

[40] R. L. C. Flemmer, C.L. Banks, On the drag coefficient of a sphere, Powder Technol. 48 (1986) 217-221.

[41] M. S. Parmar, A. N. Hayhurst, The heat transfer coefficient for a freely moving sphere in a bubbling fluidized bed, Chem. Eng. Sci. 57 (2002) 3485-3494.

[42] F. D. Natale, A. Lancia, R. Nigro, A single particle model for surface-to-bed heat transfer in fluidized beds, Powder Technol. 187 (1) (2008) 68-78.

[43] O. Molerus, A. Burschka, S. Dietz, Particle migration at solid surfaces and heat transfer in bubbling fluidized beds—I. Particle migration measurement systems, Chem. Eng. Sci. 50 (5) (1995) 871-877.

[44] J. S. M. Botterill, A. O. O. Denloye, Gas convective heat transfer to packed and fluidized beds, AIChE Symp. Ser. 176 (1978) 194-202

[45] D. Kunii, O. Levenspiel, Fluidization Engineering, 2nd ed., Butterworth-Heinemann, Newton, MA, 1991, 325.26

[46] A. P. Baskakov. Determination of the convective component of the heat transfer coefficient to a gas in a fluidized bed, Int. Chem. Eng. 12 (2) (1972) 324-326.

[47] P. Basu, Combustion and gasification in fluidized beds. Taylor & Francis Group, 2006.

[48] A. Blaszczuk, M. Pogorzelec, T. Shimizu. Heat transfer characteristics in a large-scale bubbling fluidized bed with immersed horizontal tube bundles, Energy 162 (2018) 10-19.

Journal Pre-proofs

Declaration of interests

The authors declare that they have no known competing financial interests or personal relationships that could have appeared to influence the work reported in this paper.

The novelty of the paper is indicated by the following five highlights:

- O_2/H_2O combustion of single char particles were studied in a transparent FB reactor
- Particle temperature was measured in-situ by two-color pyrometry and thermocouple
- Char temperature and burnout time of O_2/H_2O condition were lower than air condition
- The char gasification in O_2/H_2O combustion is critical and cannot be neglected
- O_2/H_2O combustion vs. various operating parameters were studied systematically

Journal Pre-proofs



https://dspace.org/

Experimental study of a single char particle combustion characteristics in a fluidized bed under O2/H2O condition

Li, Lin; Duan, Lunbo; Yang, Zhihao; Tong, Shuai; Anthony, Edward J. ...

2019-09-23
Elsevier
https://doi.org/10.1016/j.cej.2019.122942
Li L, Duan L, Yang Z, et al., (2019) Experimental study of a single char particle combustion characteristics in a fluidized bed under O2/H2O condition. Chemical Engineering Journal, Volume 382, February 2020, Article number 122942

Downloaded from a DSpace repository. https://dspace.org/